JOURNAL OF GUIDANCE, CONTROL, AND DYNAMICS
Vol. 23, No. 6, November–December 2000

Identification and Retuning of Optimum Delayed Feedback Vibration Absorber

Nader Jalili*
Northern Illinois University, DeKalb, Illinois 60115
and
Nejat Olgac†
University of Connecticut, Storrs, Connecticut 06269

A recursive system identification and retuning methodology is presented for a recently developed delayed feedback vibration absorber. The retuning is needed against the parametric variations in the system. It is performed to maintain optimal vibration suppression properties for wideband excitations. The optimized absorber offers minimum peak frequency response within the given wideband frequency range. A new scheme is introduced for the tuning of the absorber as the system experiences structural variations. The scheme suggests a nested procedure of two optimization steps, one for identification and the other for control. Feasibility of the proposed methodology is demonstrated through simulations. One of the examples deals with a single-degree-of-freedom system, and the second one is for a two-degree-of-freedom setting. Results show that with only three iterations used for the first example and five iterations used for the second example in the parameter identification part of the process, the frequency response peaks are reduced by 25%.

I. Introduction

THE tuned vibration absorber (TVA) is a passive device that reduces undesirable vibrations in the mechanical structures in the vicinity of its peak response frequency ω_{peak} (Ref. 1). It is elastically connected to the primary structure (the original vibrating mechanical structure) and properly sensitized to absorb the vibratory energy at a given frequency. When the primary structure is subjected to a wideband frequency forcing, however, the passive absorber fails to function effectively. In such cases, optimally tuned vibration absorbers with ideal structural parameters are used.[2–5] A commonly accepted optimization criterion is to minimize the peak response of the system to wideband excitation.

An example of an actively controlled TVA is, so called, the delayed resonator (DR) of Refs. 6 and 7. It uses a proportional time-delayed partial state (position, velocity, or acceleration) feedback control, on a conventional passive mass–spring–damper trio (Fig. 1). This feedback places the dominant characteristic roots of the absorber subsection on the imaginary axis, which, in turn, creates a resonant absorber. This absorber suppresses oscillations perfectly at this frequency, but at the cost of substantially worsening absorption properties at the neighboring frequencies. For wideband excitation cases, this feature is not desirable.

An improvement was made on the DR absorber to introduce a frequency response that is flat through a wide frequency range.[8] The final product is called the delayed feedback vibration absorber (DFVA). This is achieved by properly selecting the control parameters involved (feedback gain g and time delay τ in Fig. 1), as summarized later. The objective here is to introduce further improvement by performing this optimization online as the system properties show variations. Note that the variations of both the primary and the absorber are taken into account. The optimum DFVA is arrived at through the utilization of all of this information.

Earlier work on the DFVA falls short of bringing a satisfactory procedure for an online determination of feedback parameters g and τ (see Ref. 8). The main obstacles are the structural variations occurring in the system (again both in the primary and the absorber), while the DFVA suppression is in progress. An online tuning mechanism is needed to account for these variations, as in the procedure presented in Ref. 9, except that the latter treats problems with single frequency excitations. Their robust tuning process requires only the accelerations of the absorber mass and the base of DR, that is, the point of attachment. A simplification of this procedure is the truly decoupled nature of the control from the primary system properties. Thus, physical changes in the primary system play no role in the selection of control. Although this is a very effective method, the single frequency restriction introduces limitations for practical applications. The present work eliminates this limitation by treating wideband frequency cases. This objective constitutes the primary motivation for this report.

We present here a quasi-online tuning of the control parameters g and τ for optimum DFVA, in which some segments of the data are used for identification and some future data are utilized for control optimization, and so on. An iterative identification procedure is followed for the uncertain parameters of the system. An online optimization is then performed based on the newly determined parameters for the feedback gain g and time delay τ. This introduces a nested procedure, which is repeated over time as the new data become available. We then demonstrate the feasibility of this scheme through simulations.

The paper is arranged as follows: In the section immediately following the problem statement, the effect of parametric uncertainties, and the main objectives of this study are described. For simplicity we consider a single-degree-of-freedom (SDOF) primary system at this stage. Section III briefly reviews the optimization process over the control parameters g and τ with associated stability and physical constraints. The identification part is addressed in Sec. IV. Section V extends the modeling efforts to multi-degree-of-freedom (MDOF) primary structures. The two procedures described in Secs. III and IV are combined into a nested form in Sec. VI. The numerical examples are given in Sec. VII for an SDOF as well as two-degree-of-freedom (2DOF) systems.

II. Problem Statement

In this section we present a brief review of the DFVA methodology of Ref. 8. An SDOF primary system is taken into consideration to avoid undue complications in modeling. The DFVA is appended to the primary structure, and the resulting combined system is depicted in Fig. 2. Delayed acceleration feedback is considered for the absorber subsection as

$$g\ddot{x}_a(t-\tau) \tag{1}$$

Received 21 September 1998; revision received 25 August 1999; accepted for publication 24 February 2000.

*Assistant Professor, Department of Mechanical Engineering; currently Assistant Professor, Department of Mechanical Engineering, Clemson University, 205 Fluor Daniel Engineering Building, Clemson, South Carolina, 29634-0921. Member AIAA.

†Professor, Department of Mechanical Engineering; olgac@uconnvm.uconn.edu.

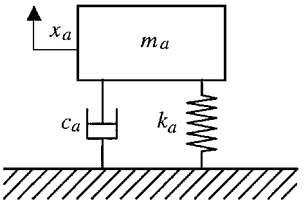

Fig. 1a Passive absorber.

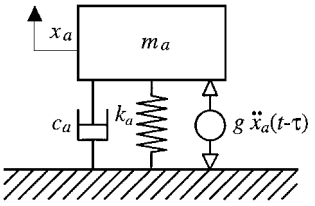

Fig. 1b Absorber with delayed acceleration feedback.

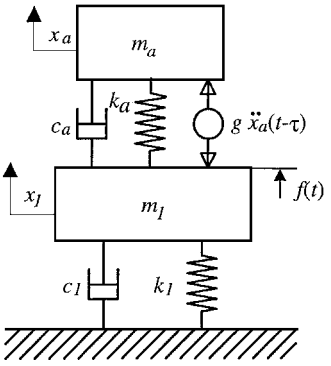

Fig. 2 DFVA on an SDOF primary system.

where g and τ are the feedback gain and time delay, respectively. Here, the control parameters g and τ are selected for properly placing the dominant poles of the combined system. This is different than the delayed resonator (DR) strategy, where the dominant poles of the absorber are on the imaginary axis. For the reader's convenience, a brief overview of the DR concept is presented in Appendix A.

The equations of motion governing the dynamics of Fig. 2 are

$$m_a\ddot{x}_a(t) + c_a\dot{x}_a(t) + k_a x_a(t) - g\ddot{x}_a(t-\tau) = c_a\dot{x}_1(t) + k_a x_1(t) \tag{2}$$

$$m_1\ddot{x}_1(t) + (c_1 + c_a)\dot{x}_1(t) + (k_1 + k_a)x_1(t) - \{c_a\dot{x}_a(t) + k_a x_a(t) - g\ddot{x}_a(t-\tau)\} = f(t) \tag{3}$$

where $x_1(t)$ and $x_a(t)$ are the respective primary and absorber displacements and $f(t)$ is a wideband excitation force. We define a vector $\boldsymbol{\theta} = \{m_a\ c_a\ k_a\ m_1\ c_1\ k_1\}^T$ of the system parameters whose components are indicated in Fig. 2.

It is assumed that the true value of $\boldsymbol{\theta}$, for instance, $\boldsymbol{\theta}^*$, is unknown, but bounded. That is,

$$\|\Delta\boldsymbol{\theta}/\bar{\boldsymbol{\theta}}\| \le \psi \tag{4}$$

where $\|\|$ denotes a vector norm, / represents a term-by-term division, ψ is a positive finite scalar,

$$\Delta\boldsymbol{\theta} = \boldsymbol{\theta}^* - \bar{\boldsymbol{\theta}} = \begin{cases} \Delta m_a = m_a^* - \bar{m}_a \\ \Delta c_a = c_a^* - \bar{c}_a \\ \Delta k_a = k_a^* - \bar{k}_a \\ \Delta m_1 = m_1^* - \bar{m}_1 \\ \Delta c_1 = c_1^* - \bar{c}_1 \\ \Delta k_1 = k_1^* - \bar{k}_1 \end{cases} \tag{5}$$

Here, $(\,)^*$ and $\bar{(\,)}$ denote the respective true and nominal values of the argument.

The Laplace domain representation of the system of Eqs. (2) and (3) is

$$\left(m_a s^2 + c_a s + k_a - g s^2 e^{-\tau s}\right)X_a(s) = (c_a s + k_a)X_1(s)$$

$$\left\{m_1 s^2 + (c_1 + c_a)s + (k_1 + k_a)\right\}X_1(s) - \left(c_a s + k_a - g s^2 e^{-\tau s}\right)X_a(s) = F(s) \tag{6}$$

where $X_a(s)$, $X_1(s)$, and $F(s)$ are the Laplace transformations of $x_a(t)$, $x_1(t)$, and $f(t)$, respectively. The transfer function between the excitation force and primary system acceleration is then written as

$$\mathrm{TF}(s) = \frac{s^2 X_1(s)}{F(s)} = s^2\left\{\frac{m_a s^2 + c_a s + k_a - g s^2 e^{-\tau s}}{H(s)}\right\} \tag{7}$$

where

$$H(s) = \left\{m_1 s^2 + (c_1 + c_a)s + k_1 + k_a\right\}\left(m_a s^2 + c_a s + k_a - g s^2 e^{-\tau s}\right) - (c_a s + k_a)\left(c_a s + k_a - g s^2 e^{-\tau s}\right)$$

Notice that the characteristic equation of the combined system is simply

$$H(s) = 0 \tag{8}$$

For each $g \neq 0$ and $\tau \neq 0$, Eq. (8) has infinite number of roots, which are called the spectrum of the time-delayed system. The passive absorber, that is, $g = 0$, is always stable, whereas a DFVA with improper selection of gain and delay can drive the system to instability. Naturally, the stability requirement has to be satisfied throughout the search of optimal control.

A. Optimization over Control Parameters

The principle objective of this study is to find the control parameters g and τ such that the peak magnitude of the frequency transfer function (FTF)

$$J = \max\{|\mathrm{FTF}(\omega)|\} = \max\{|\mathrm{TF}(s)|_{s=j\omega}\}, \qquad j = \sqrt{-1} \tag{9}$$

is minimized over a prescribed wideband frequency range. The numerical problem is, therefore, to minimize J over g and τ, subject to some constraints. The results are obviously dependent on the system properties at hand. Therefore, the variations in the structural parameters of the system should be accounted for. The approach to obtain the optimal feedback control is, hence, mixed with the application of system identification in a sequential manner.

B. Identification Objective

An identification scheme should provide the best estimates of the system parameters θ^*. For a time-varying system, this needs to be done online. As the system parameters show variation, the corresponding feedback control optimization should follow. This scheme lends itself to a nested identification/optimization procedure as described in the following section.

III. Optimization over the Control Parameters

For this process, we assume the structural properties are fixed and known. In principle, this optimization is similar to that of Ref. 8. Here, we review the procedure for clarity. The objective of the optimization is to minimize the peak frequency response of the system over a wide frequency band. It has been shown in the literature that both flattening the frequency response and minimizing its peak yield the same result.[4,10,11]

The procedure is a min-max operation: Find the control parameters g and τ that minimize the peak frequency response $\mathrm{FTF}(\omega)$ of the primary system. In other words, we seek the optimal solution to

$$\min_{g,\tau}\left\{\max_{\omega_{\mathrm{low}} \le \omega \le \omega_{\mathrm{up}}} [\mathrm{FTF}(g, \tau, \omega)]\right\} \tag{10}$$

subject to the constraints $g, \tau > 0$, and the assurance of the system stability.

During various steps of searching for the optimal solution, g and τ selections should remain in the stable region. For a given system, this region on the g, τ plane is well defined, although its description may be numerically complex (Refs. 12 and 13).

A. Stability of the Feedback Control

Let us take the characteristic Eq. (8) of the combined system and recast into the form

$$ge^{-\tau s} = \frac{m_1 m_a s^4 + (m_a c_1 + m_a c_a + m_1 c_a)s^3 + (m_a k_1 + m_a k_a + m_1 k_a + c_1 c_a)s^2 + (k_1 c_a + c_1 k_a)s + k_1 k_a}{s^2\left(m_1 s^2 + c_1 s + k_1\right)} = \frac{N(\boldsymbol{\theta}, s)}{D(\boldsymbol{\theta}, s)} \tag{11}$$

The necessary and sufficient condition for asymptotic stability is that the roots of the characteristic Eq. (11), all have negative real parts. This equation is transcendental and presents infinitely many finite roots. Therefore, the verification of the root locations is not a trivial task. We revisit a stability chart strategy as described in Ref. 12.

When the combined system is marginally stable, there are at least two roots of the characteristic equation on the imaginary axis, that is, $s = \pm j\omega_{cs}$, where subscript cs denotes the combined system. The introduction of this condition into Eq. (11) yields the necessary control parameters:

$$g_{cs} = \left| \frac{N(\boldsymbol{\theta}, \omega_{cs} j)}{D(\boldsymbol{\theta}, \omega_{cs} j)} \right| \tag{12}$$

$$\tau_{cs} = \frac{1}{\omega_{cs}} \left\{ (2\ell - 1)\pi + \angle \frac{N(\boldsymbol{\theta}, \omega_{cs} j)}{D(\boldsymbol{\theta}, \omega_{cs} j)} \right\}, \qquad \ell = 1, 2, \ldots \tag{13}$$

where $|\,|$ and $\angle$ are the magnitude and the angle of the arguments, respectively.

For a particular delay $\tau = \tau_0$, the combined system crossings $\omega_{cs\ell}(\tau_0)$ are determined from Eq. (13) and corresponding gains $g_{cs\ell}$ from Eq. (12), where the subscript and counter $\ell = 1, 2, \ldots$ refer to the first, second, etc., root loci branch crossings. To ensure stability of the system, the feedback gain g should be smaller than the minimum of these $g_{cs\ell}(\omega_{cs\ell})$ values. That is,

$$g < g_{\min}[\omega_{cs\ell}(\tau_0)] \tag{14}$$

where

$$g_{\min} = \min \begin{Bmatrix} g_{cs}(\omega_{cs1}) \\ g_{cs}(\omega_{cs2}) \\ g_{cs}(\omega_{cs3}) \\ \vdots \end{Bmatrix} \tag{15}$$

for $\tau = \tau_0$. These operating points, $\{\min g_{cs\ell}, \tau_{cs\ell}\}$, $\ell = 1, 2, \ldots$, form the marginal stability boundary for the combined system, below which (i.e., $g_{cs} < \min g_{cs\ell}$) the system is stable, and above which it is unstable. This judgment follows the D-subdivision rule explained in Refs. 14 and 15 and applied for DR stability analysis in Ref. 13. A typical outlook of such a curve is depicted in Fig. 3. The stability boundary between the infeasible and feasible regions is numerically determined using Eq. (15).

B. Constrained Optimization Strategy

For the determination of optimal control parameters, the structural properties are assumed fixed. The proposed constrained optimization problem is then cast in the form

$$J_{DFVA} = \min_{g,\tau} \left\{ \max_{\omega_{low} \le \omega \le \omega_{up}} [\mathrm{FTF}(g, \tau, \omega)] \right\} = \min_{g,\tau} \{G_{DFVA}(g, \tau)\} \tag{16}$$

subject to physical bounds

$$h_1 \equiv -g < 0, \qquad h_2 \equiv -\tau < 0 \tag{17}$$

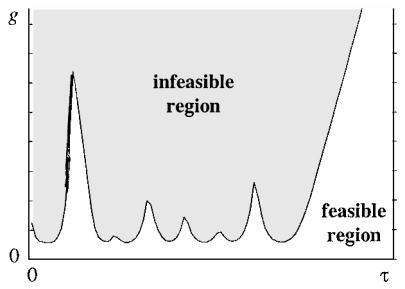

Fig. 3 Typical feasible region for the control parameters.

and the stability constraint

$$h_3 \equiv g - g_{\min} < 0 \tag{18}$$

A typical feasible region dictated by the constraints (17) and (18) is again depicted in Fig. 3. G_{DFVA} in Eq. (16) is the peak of the FTF.

The initial control parameters g and τ are estimated to start the process. A rational starting point is the corresponding DR feedback gain g_c and time delay τ_c at the resonance frequency of the primary structure ω_{peak}. That is, the initial g and τ are taken as g_c and τ_c of Eq. (A5) with the designated frequency $\omega_c = \omega_{peak}$.

The optimum values of g and τ are numerically determined next, according to the descriptions in Eqs. (16–18). Because the computation of the derivatives of the objective function $G_{DFVA}(g, \tau)$ is very complicated, we seek an optimization technique that uses inferior information. For this, the direct update methods are considered. These methods require the computation of only the first derivatives of the cost function. In this procedure, the information obtained from earlier iterations is used to accelerate the convergence towards the minimum. Here, we use a widely accepted version of direct update methods, the Broyden–Fletcher–Goldfarb–Shanno (BFGS) routine, which has been proven to be most effective in similar applications (see Ref. 16 and a brief summary in Appendix B).

IV. Recursive Identification of the System Parameters

Assume that the initial control parameters g and τ are determined using the nominal plant parameters. This initiates the vibration absorption operation. The variations in the structural parameters, however, are not yet considered. A strategy is described in this section for the determination of these variations.

A. Performance Specification

A method that uses only absorber acceleration is presented here. This signal should be sufficient to identify the parametric variations in the structure. Imagine that an excitation $f(t)$ and the control with g and τ are applied to both the true plant (or experimental setup) and the nominal plant, as shown in Fig. 4. $G_P^*(\boldsymbol{\theta}^*)$ and $G_P(\boldsymbol{\theta})$ are the transfer operators of the true and the model plants, respectively, and $C(g, \tau)$ is the control law given in Eq. (1).

The objective of the parameter identification is to minimize the difference between true absorber acceleration output $\ddot{x}_a^*(t)$ and nominal absorber acceleration output $\ddot{x}_a(t)$ by proper selection of the system parameters $\boldsymbol{\theta}$. The problem can be stated with a cost function

$$J_{ID} = \min_{\theta} \left\{ \left\| \ddot{x}_a^*(t, \boldsymbol{\theta}^*) - \ddot{x}_a(t, \boldsymbol{\theta}) \right\| \right\} = \min_{\theta} \{G_{ID}(\boldsymbol{\theta})\} \tag{19}$$

subject to the physical constraint

$$\boldsymbol{\theta} > \mathbf{0} \tag{20}$$

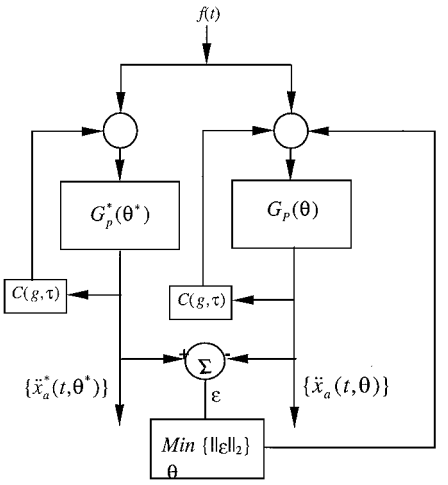

Fig. 4 Schematic of the identification objective.

and the inequality bound

$$\|\boldsymbol{\theta}/\bar{\boldsymbol{\theta}} - \mathbf{1}\| \leq \psi \tag{21}$$

The nominal absorber acceleration is obtained by solving differential Eqs. (2) and (3) with nominal parameters, $\boldsymbol{\theta} = \bar{\boldsymbol{\theta}}$. It is also assumed that $\bar{\boldsymbol{\theta}}$ satisfies inequality (4). The parameter $\boldsymbol{\theta}$ is then numerically updated in such a way that the cost function described in Eq. (19), subject to constraints (20) and (21), is minimized. The same method of optimization discussed in Sec. III is used, which guarantees the convergence of $\boldsymbol{\theta}$ to its true value $\boldsymbol{\theta}^*$ as described next.

B. Convergence of the Parameters

The initial guess $\boldsymbol{\theta} = \bar{\boldsymbol{\theta}}$ for the optimization process satisfies constraints (20) and (21). For a procedural simplification, the constrained optimization problem of Eqs. (19–21) can be converted to an unconstrained optimization problem with a transformation described in Appendix B. That is, problem

$$J_{\mathrm{ID}} = \min_{\theta}\{G_{\mathrm{ID}}(\boldsymbol{\theta})\} \tag{22}$$

subject to inequality constraints

$$h_1^{\mathrm{ID}} \equiv -\boldsymbol{\theta} < \mathbf{0}, \qquad h_2^{\mathrm{ID}} \equiv \|\boldsymbol{\theta}/\bar{\boldsymbol{\theta}} - \mathbf{1}\| - \psi \leq 0 \tag{23}$$

is converted into the unconstrained problem

$$G_{\mathrm{ID,new}}(\boldsymbol{\theta}, \boldsymbol{r}) = G_{\mathrm{ID}}(\boldsymbol{\theta}) + Q[\boldsymbol{h}(\boldsymbol{\theta}), \boldsymbol{r}] \tag{24}$$

where $\boldsymbol{r}$ is a vector of penalty imposing parameters. Q is a real-valued function whose contribution to the objective function ($G_{\mathrm{ID,new}}$) is controlled by $\boldsymbol{r}$. The form of this additional penalty can be appropriately selected. Here we use the inverse barrier function of Ref. 17:

$$Q[\boldsymbol{h}(\boldsymbol{\theta}), r] = \left(\frac{1}{r}\right)\sum_{i=1}^{2}\left[\frac{-1}{h_i(\boldsymbol{\theta})}\right] \tag{25}$$

where r is taken as a positive scalar. It is clear that as the parameter $\boldsymbol{\theta}$ gets closer to the constraint, h_i becomes smaller, increasing the value of Q rapidly.

The function Q becomes infinite if any one of the inequality boundaries becomes active. Thus, if the iterative process starts from a feasible point, it does not go into the infeasible region because of the huge barrier. It is shown that as $r \to \infty$, that is, as $Q \to 0$, $\boldsymbol{\theta}^*_{\mathrm{new}} \to \boldsymbol{\theta}^*$ and the minimum of the objective function $G_{\mathrm{ID,new}}(\boldsymbol{\theta}, r)$ is reached. The $\boldsymbol{\theta}^*$ is the optimum solution of the original constrained optimization problem.

V. Extension to MDOF Primary Structures

Parameter identification and optimal absorber treatment can be extended to cases with MDOF primary systems. The resulting combined system, the DFVA appended on this MDOF primary structure, is depicted in Fig. 5. The DFVA is attached on the qth mass (or DOF) of the primary structure. It is desired, again, to minimize the peak frequency response of the qth mass, on the primary system, for a given wideband frequency interval.

The state-space representation of this system is written in the form of linear simultaneous differential equations:

$$\dot{\boldsymbol{y}}(t) = \boldsymbol{A}_0\boldsymbol{y}(t) + g\boldsymbol{A}_\tau\dot{\boldsymbol{y}}(t-\tau) + \boldsymbol{f}(t) \tag{26}$$

where

$$\boldsymbol{y}(t) = \{\underbrace{x_1, \dot{x}_1, \ldots, x_n, \dot{x}_n}_{2n}, x_a, \dot{x}_a\}^T$$

$$\boldsymbol{f}(t) = \{\underbrace{0, f_1, \ldots, 0, f_n}_{2n}, 0, 0\}^T \in \Re^{2(n+1)\times 1}$$

are the state variable and excitation vectors. The displacements of the primary structure and the absorber are denoted by $x_i(t)$, where $i = 1, 2, \ldots, n$, and $x_a(t)$, respectively. $\boldsymbol{A}_0$ and $\boldsymbol{A}_\tau \in \Re^{2(n+1)\times 2(n+1)}$ are the constant system matrices.

The Laplace domain representation of the system is written in general form as

$$\left(s\boldsymbol{I} - \boldsymbol{A}_0 - gse^{-\tau s}\boldsymbol{A}_\tau\right)\boldsymbol{Y}(s) = \boldsymbol{H}(s)\boldsymbol{Y}(s) = \boldsymbol{F}(s) \tag{27}$$

and the corresponding characteristic equation is

$$|\boldsymbol{H}(s)| = \det\left[s\left(\boldsymbol{I} - ge^{-\tau s}\boldsymbol{A}_\tau\right) - \boldsymbol{A}_0\right] = 0 \tag{28}$$

To not divert the focus of this study, we leave the details of this derivation to Ref. 8. For this paper, it is sufficient to say that the primary structure acceleration on the qth mass $s^2X_q(s)$ is functionally linked to the excitation force and control as shown in Fig. 5. The frequency transfer function between the external force at point p and the acceleration $\ddot{x}_q$ is

$$\mathrm{FTF}_q(\omega) = \left|\frac{s^2X_q(s)}{F_p(s)}\right|_{s=j\omega} \begin{cases} p: p\text{th mass} \\ q: q\text{th mass} \end{cases} \tag{29}$$

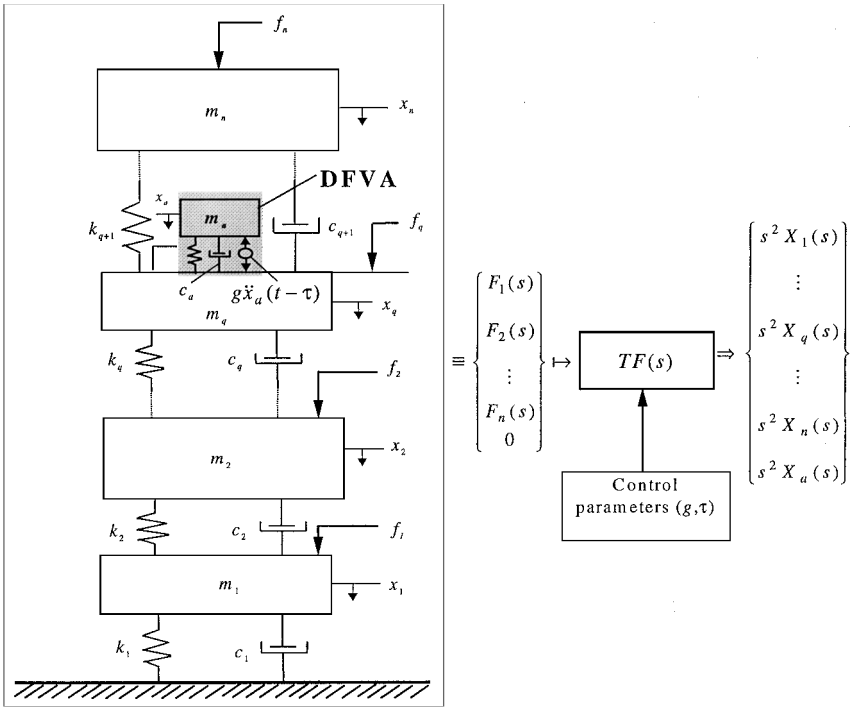

Fig. 5 DFVA implementation on an *n*DOF structure.

A. Optimization on the Control Parameters

Based on the same arguments presented in Sec. III.A, the feedback gain g should be smaller than the infemum of the $g_{cs,\ell}$, $\ell = 1, 2, \ldots$, to ensure stability of the system. To construct the stability boundaries, the characteristic Eq. (28) of the combined system is rewritten leaving $ge^{-\tau s}$ term on the left-hand side, as in Eq. (11). The procedure described in Sec. III.A is then followed.

The constrained optimization problem is written in parallel to Eq. (16),

$$J_{\mathrm{DFVA}} = \min_{g,\tau}\left\{ \max_{\omega_{\mathrm{low}} \le \omega \le \omega_{\mathrm{up}}} [\mathrm{FTF}_q(g, \tau, \omega)] \right\} = \min_{g,\tau}\{G_{\mathrm{DFVA}}(g, \tau)\} \tag{30}$$

subject to constraints (17) and (18). The min-max problem is solved for g and τ as described in Sec. III.B with one difference: The expressions contain a higher number of terms due to the added DOF.

B. Parameter Identification

With the same discussion presented in Sec. IV.A, the absorber acceleration is used in the identification part. Through the governing equation (27), the absorber acceleration is obtained as

$$\ddot{x}_a(t) = \mathcal{L}^{-1}\left\{s^2 X_a(s)\right\} \tag{31}$$

The objective of identification is to minimize Eq. (19) subject to the constraints (20) and (21). The absorber acceleration of Eq. (31) is used in the objective function (19) with the new system parameters $\boldsymbol{\theta} = \{m_a \;\; c_a \;\; k_a \;\; m_1 \;\; c_1 \;\; k_1 \;\; \cdots \;\; m_n \;\; c_n \;\; k_n\}^T$, which represent an extended form of $\boldsymbol{\theta}$ given in Sec. II.

VI. Nested Optimum Feedback Control and Identification

The two optimization processes described earlier (one for identification and the other for vibration absorption) are combined. We assume that the nominal system parameters are available and satisfy inequality (4). It is also assumed that the absorber acceleration is available as measured data. An offline optimization over the control parameters g and τ using the nominal system parameters $\bar{\boldsymbol{\theta}}$ is performed first. We denote this set of optimum control parameters by $\bar{g}$ and $\bar{\tau}$.

To identify the system parameters $\boldsymbol{\theta}$ corresponding to the measured data, that is, the absorber acceleration, we freeze a segment of the data and implement the system identification optimization. This step is followed by the optimization on g and τ based on the newly identified parameters. The number of iterations for each optimization is controlled such that the execution time is kept below a certain value. This duration can be appropriately selected by the user. For instance, if the process at hand is a bridge oscillation and the parametric variations do not occur faster than once each hour, the two optimizations mentioned may be allowed to run in the order of minutes.

As soon as the new control parameters become available they are implemented on the true plant (experimental setup), and a new segment of data is collected to repeat this procedure. Because the convergence toward the true system parameters $\boldsymbol{\theta}^*$ is guaranteed, this repetition improves the quality of the identification. Figure 6 depicts the flow chart of this methodology. The duration of T_c is determined by the speed of the processor involved and may change at each iteration depending on the data set processed. The speed of variation of system parameters $\boldsymbol{\theta}$, however, will have to be slower than the computational time needed for their identification.

Note that the stability constraint, expression (18), varies simultaneously in each iteration of identification. This procedure is included in the optimization loop, as shown in Fig. 6.

VII. Numerical Examples and Results

To demonstrate the effectiveness of the proposed identification/optimization structure, two examples are presented. First, we consider a simple SDOF system to explain the nested parameter identification/optimized control scheme and to highlight its features. In the second example, a more complex 2DOF system with DFVA attached to the upper mass is studied to demonstrate the feasibility of the method for higher DOF primary structures.

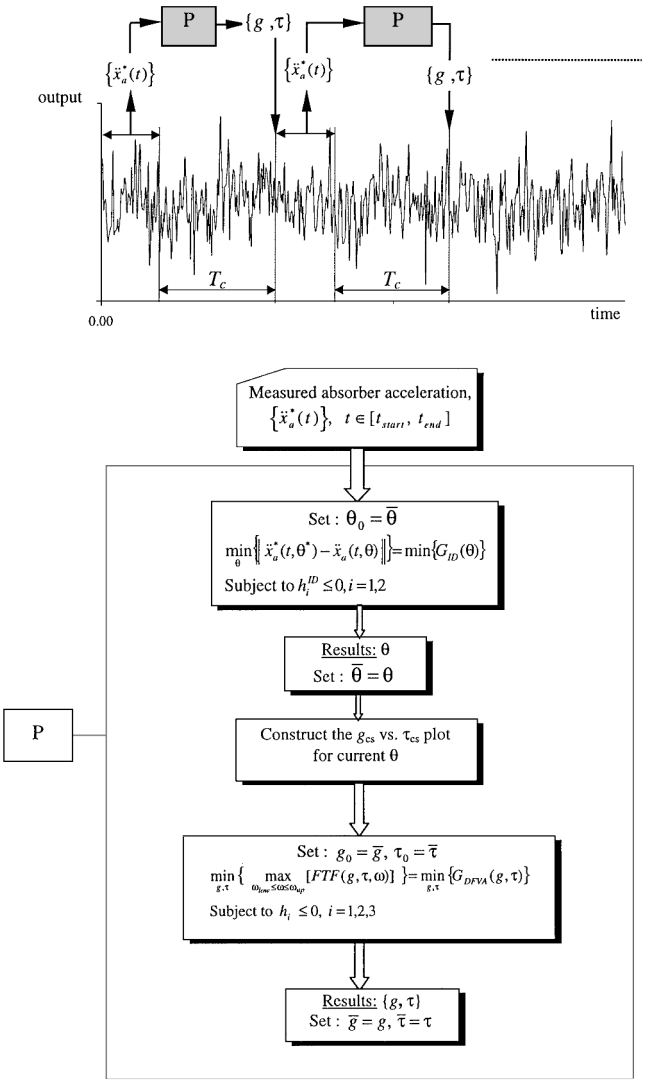

Fig. 6 Flow chart for the nested optimization procedure (P stands for optimization process).

A. DFVA Implementation on SDOF Structure

The SDOF structure of Fig. 2 is taken as the first example. We consider step-type variations on the parameters k_a, c_a, k_1, and c_1 from their nominal (estimated) values, $\bar{k}_a$, $\bar{c}_a$, $\bar{k}_1$, and $\bar{c}_1$. It is clear that variations in these parameters are likely to happen much more frequently than those of m_a and m_1. Therefore, the masses are taken as time-invariant quantities. For a numerical example, we assume that the nominal values are arbitrarily perturbed as

$$\begin{aligned} k_a^* &= 1.10\bar{k}_a, & c_a^* &= 1.10\bar{c}_a \\ k_1^* &= 1.05\bar{k}_1, & c_1^* &= 1.05\bar{c}_1 \\ m_a^* &= \bar{m}_a, & m_1^* &= \bar{m}_1 \end{aligned} \tag{32}$$

with the primary system parameters of

$$\begin{aligned} \bar{m}_1 &= 5.77 \text{ kg}, & \bar{k}_1 &= 251.132 \times 10^6 \text{ N/m} \\ \bar{c}_1 &= 197.92 \text{ kg/s}, & \bar{m}_a &= 0.227 \text{ kg} \end{aligned} \tag{33}$$

It is concluded that setting the absorber stiffness and damping (k_a and c_a) free during the optimization iterations offers a significant improvement over keeping them fixed, even if these fixed values were that of the optimum passive absorber's.[8] We present the numerical results in the following progression:

1) The optimum setting for the DFVA absorber subsection is searched first, based on the nominal primary system. The

constrained optimization over $[k_a, c_a, g, \tau]^T \in \Re^4$ is performed. This procedure yields the optimal absorber

$$k_a^{\text{opt}} = \bar{k}_a = 9.8014 \times 10^6 \text{ N/m}, \qquad c_a^{\text{opt}} = \bar{c}_a = 35.48 \text{ kg/s}$$

$$g_{\text{opt}} = \bar{g} = 0.0424 \text{ kg}, \qquad \tau_{\text{opt}} = \bar{\tau} = 0.7305 \text{ ms} \tag{34}$$

2) These starting values are used next for the nested parameter identification/control optimization process as per the flow chart in Fig. 6. A typical time trace of the true primary acceleration is shown in Fig. 7. Notice that this time history is obtained using the perturbed parameters as in Eq. (32), which are to be recovered. The iteration results are shown in Table 1, which demonstrate the convergence of all parametric uncertainties in just three steps. To display the improvement on the frequency response, the true frequency transfer function (9) along with the discrete Fourier spectra of the measured data are shown in Fig. 8. The discrete Fourier spectra, Fig. 8b, is obtained as

$$\text{DFS}(\omega_k) = \left| \frac{X_{\text{DFT}}(\omega_k)}{F_{\text{DFT}}(\omega_k)} \right| \tag{35}$$

where

$$\omega_k = \frac{2\pi k}{NT_s}, \qquad X_{\text{DFT}}(\omega_k) = \sum_{n=0}^{N-1} \ddot{x}_p(nT_s) e^{-jn\omega_k T_s}$$

$$F_{\text{DFT}}(\omega_k) = \sum_{n=0}^{N-1} f(nT_s) e^{-jn\omega_k T_s}$$

where N is the number of recorded data, and T_s is the sampling time. Notice the close correspondence of Figs. 8a and 8b from the frequency spectrum viewpoint. The optimum behavior (at the end of third step) clearly shows a flatter spectrum where the peak response is suppressed.

Notice that the excitation force $f(t)$ and the resulting primary acceleration have a wide band nature and, hence, count as nonperiodic signals. The problems associated with these signals in the frequency domain is that the ratio of the corresponding discrete Fourier spectra is not equal to the true frequency transfer function, as is obvious from Figs. 8a and 8b. That is the reason why the identification in this study is performed in the time domain. It is the common conviction that the frequency-domain system identification suffers from the drawback that it cannot handle arbitrary signals without introducing systematic errors. The aim of giving these spectra here is just to show the trend of improvement on frequency response in consecutive steps of identification.

B. DFVA Implementation on 2DOF Structure

The second example consists of a two-mass primary system with DFVA subsection mounted on the upper mass (Fig. 9). It is desired to suppress vibrations at the point of attachment of DFVA while the lower mass is being excited by a wideband disturbance. That is, the FTF between f_1 and $\ddot{x}_2$ is

$$\text{FTF}_2(\omega) = \left| \frac{s^2 X_2(s)}{F_1(s)} \right|_{s=j\omega} \tag{36}$$

One of the masses m_1 and its restoring components k_1 and c_1 are identical to those of the first example, and the remaining system properties are

$$\bar{m}_2 = 7.00 \text{ kg}, \qquad \bar{k}_2 = 350.00 \times 10^6 \text{ N/m}, \qquad \bar{c}_2 = 220.00 \text{ kg/s} \tag{37}$$

As in the first example, the four-dimensional DFVA optimization over $[k_a, c_a, g, \tau]^T \in \Re^4$ is handled first with the 2DOF primary

Table 1 Iteration steps in identification and optimization for SDOF primary

Step	J_{DFVA}	$J_{\text{ID}} \times 10^{-6}$	$g^{(k)}$, kg	$\tau^{(k)}$, ms	k_a^*/k_a	c_a^*/c_a	k_1^*/k_1	c_1^*/c_1	$100\|(\theta - \theta^*)/\theta^*\|_2$
1[a]	1.2367	139.97	0.0424	0.7305	1.1000	1.1000	1.0500	1.0500	14.51
2	0.9603	1.3142	0.0460	0.6798	1.0003	1.0311	0.9999	1.1540	13.68
3	0.9578	0.2528	0.0459	0.6795	0.9999	0.9976	1.0000	0.9958	0.48
Desired	Min$\{M_{\text{peak}}\}$	0	——	——	1.0000	1.0000	1.0000	1.0000	0

[a]Here, $\boldsymbol{\theta} = \bar{\boldsymbol{\theta}}$.

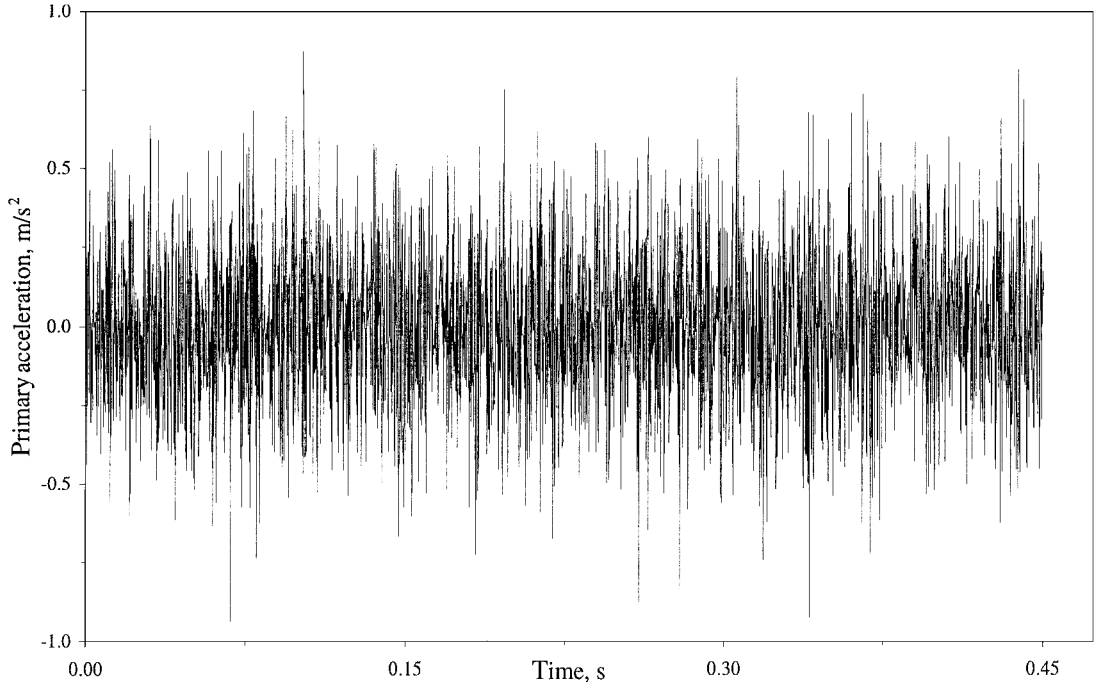

Fig. 7 Time trace of primary acceleration.

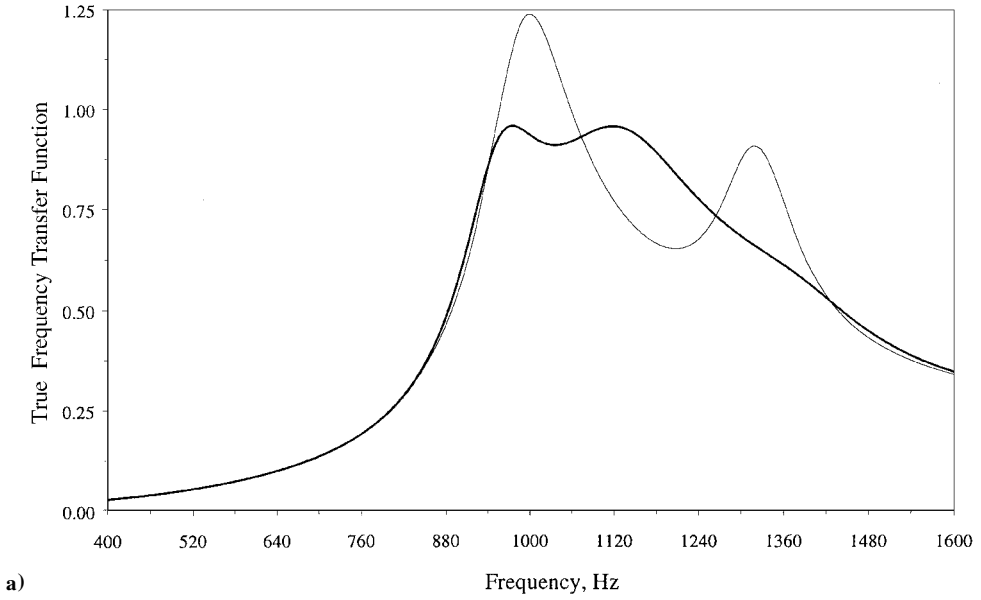

a)

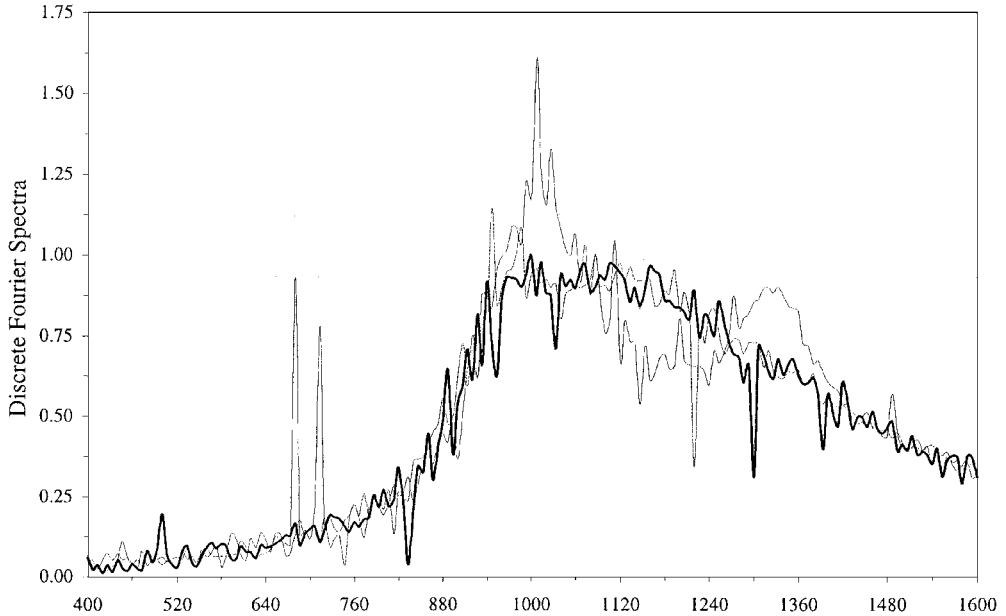

b)

Fig. 8 Comparison between true transfer functions and discrete Fourier spectra: the true system is based on the nominal control parameters, step 1 (thin-solid); one-step identification/optimization, step 2 (thin-dotted); and two-step identification/optimization, step 3 (thick-solid).

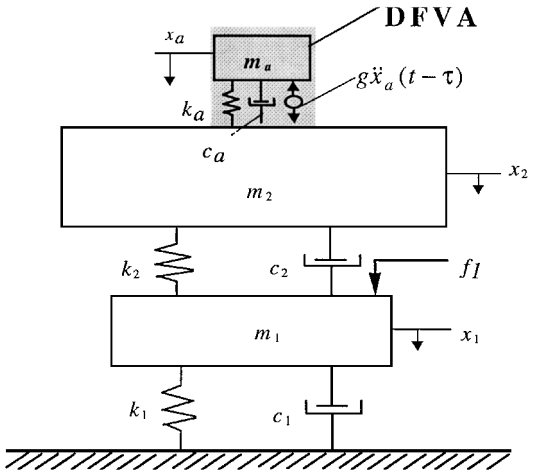

Fig. 9 DFVA on a 2DOF primary system.

properties fixed at their nominal settings. This yields an initial startup point for (g, τ) and the new optimum absorber parameters as

$$k_a^{\text{opt}} = \bar{k}_a = 9.8014 \times 10^6 \text{ N/m}, \qquad c_a^{\text{opt}} = \bar{c}_a = 1979.70 \text{ kg/s}$$
$$g_{\text{opt}} = \bar{g} = 0.1962 \text{ kg}, \qquad \tau_{\text{opt}} = \bar{\tau} = 0.0055 \text{ s} \quad (38)$$

The nominal values of absorber and lower and upper masses are then arbitrarily perturbed as

$$k_a^* = 1.10\bar{k}_a, \qquad c_a^* = 1.10\bar{c}_a$$
$$k_1^* = 1.10\bar{k}_1, \qquad c_1^* = 1.05\bar{c}_1$$
$$k_2^* = 1.05\bar{k}_2, \qquad c_2^* = 1.10\bar{c}_2$$
$$m_a^* = \bar{m}_a, \qquad m_1^* = \bar{m}_1, \qquad m_2^* = \bar{m}_2 \quad (39)$$

The proposed autotuning algorithm is again followed with the results shown in Table 2. It is observed that, in about five steps, all system parameters are identified and the peak of the frequency response (J_{DFVA}) is reduced more than 30%.

Table 2 Iteration steps in identification and optimization for 2DOF primary

Step	J_{DFVA}	J_{ID}	$g^{(k)}$, kg	$\tau^{(k)}$, s	k_a^*/k_a	c_a^*/c_a	k_1^*/k_1	c_1^*/c_1	k_2^*/k_2	c_2^*/c_2	$100\|\|(\theta-\theta^*)/\theta^*\|\|_2$
1[a]	1.4914	——	0.1962	0.0055	1.1000	1.1000	1.1000	1.0500	1.0500	1.1000	——
2	1.0961	1.3561	0.1689	0.0053	1.1198	1.0198	1.0006	1.0652	1.0014	1.0895	14.9372
3	1.0469	0.3872	0.1829	0.0053	1.0320	1.0075	1.0001	1.1673	0.9998	1.0226	14.8449
4	1.0236	0.0890	0.1885	0.0053	1.0066	1.0001	1.0000	1.1192	1.0000	0.9720	11.0505
5	1.0230	0.0009	0.1886	0.0053	1.0000	1.0000	1.0000	0.9996	1.0000	1.0001	0.0381
Desired	$\text{Min}\{M_{\text{peak}}\}$	0	——	——	1.0000	1.0000	1.0000	1.0000	1.0000	1.0000	0

[a]Here, $\theta = \bar{\theta}$.

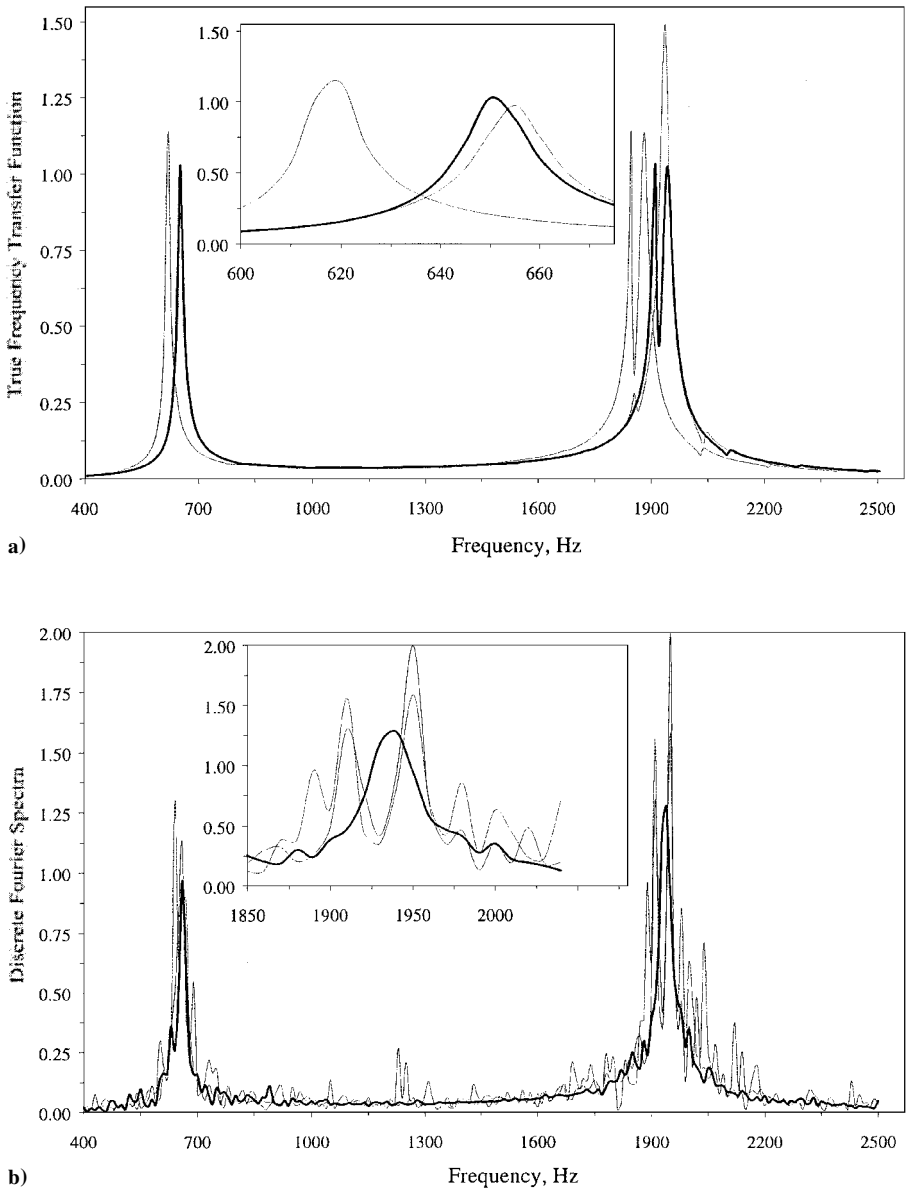

Fig. 10 Comparison between a) true transfer functions (thin-dotted, tuned DFVA; thin-solid, detuned DFVA; and thick-solid, retuned DFVA) and b) discrete Fourier spectra (thin-solid, step 1; thin-dotted, step 3; and thick-solid, step 5 as per Table 2).

The true FTF (36) and discrete Fourier spectra of the measured data are shown in Fig. 10. In contrast with Fig. 8a, we plot the tuned (nominal system with $\bar{g}$ and $\bar{\tau}$), detuned (actual system with $\bar{g}$ and $\bar{\tau}$, step 1 in Table 2), and, finally, retuned (actual system with g and τ, step 5 in Table 2) systems in Fig. 10a. The optimum operation at the end of fifth step clearly demonstrates the feasibility of the method for higher DOF primary structures as well.

The DFVA characteristics are better demonstrated at different frequencies as shown in Fig. 11. The excitation amplitude is kept at unity and its frequency is changed around the second peak of FTF (Fig. 10). This peak is selected because it shows a pronounced frequency response improvement. For Fig. 10, every 0.15 s the frequency of the excitation is changed as 1860, 1880, 1900, 1920, 1930, 1950, and 1970 Hz. The upper graph in Fig. 11 shows the response of the upper mass with a tuned DFVA setting. The largest amplitude is at 1880 Hz. When the detuning takes effect, the largest response is increased by 23% (see the middle graph). The system with a retuned DFVA shows considerable vibration suppression (about 32%) over the detuned absorber (lower graph). This is precisely the objective of the DFVA retuning scheme.

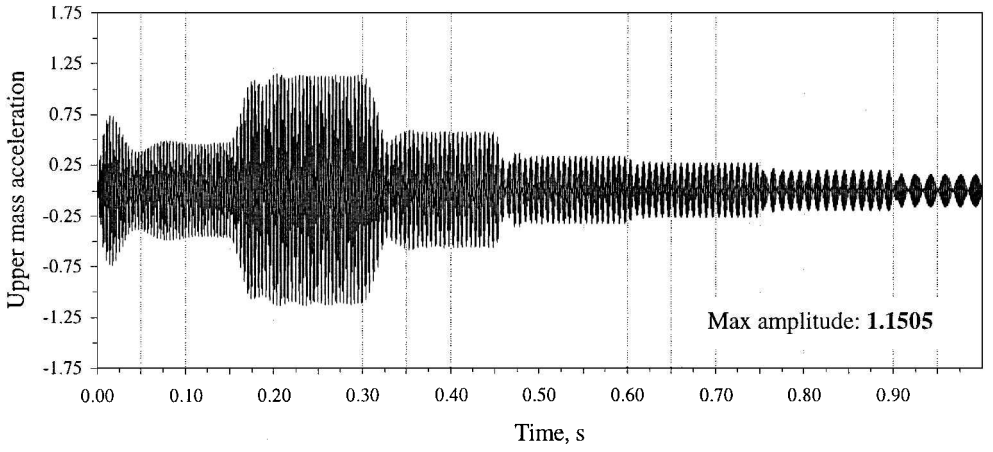

a) Tuned DFVA

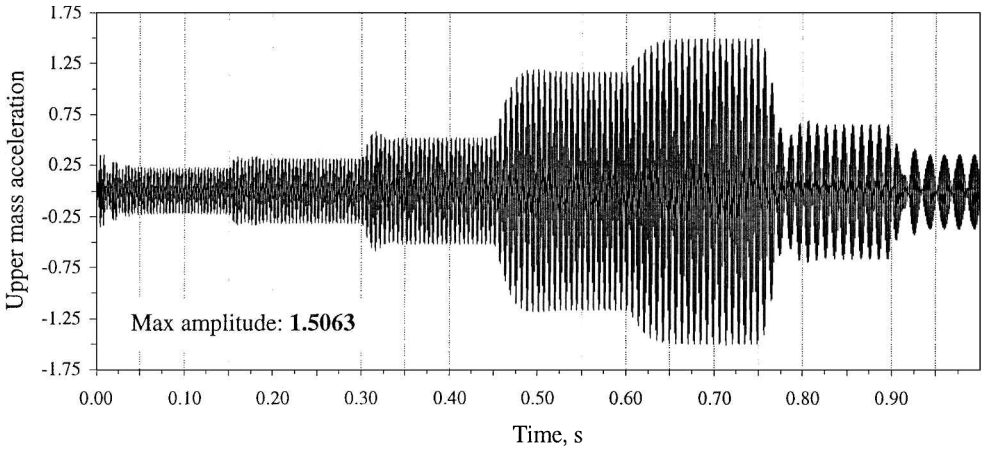

b) Detuned DFVA

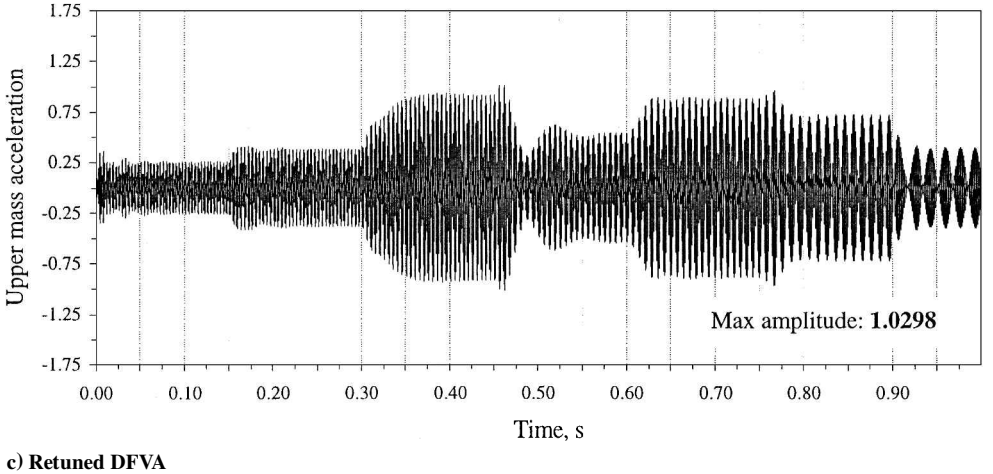

c) Retuned DFVA

Fig. 11 Frequency sweep each 0.15 s around the second peak, that is, 1860, 1880, 1900, 1920, 1930, 1950, and 1970 Hz.

VIII. Conclusions

An actively controlled absorber is used to improve the wideband frequency response of a structure. The proposed control strategy is of a very simple time-delayed partial state feedback type. An essential component of this strategy is presented in this paper, which deals with the parametric variations within the system. To increase the absorber efficiency against such variations, an identification process is utilized in sequence with an optimization for tuning the absorber. A nested quasi-real-time system identification/control process is developed to achieve this recursive operation. Example cases for SDOF and MDOF primary systems are taken into account. The performance improvement is demonstrated via simulations.

Appendix A: DR Concept Overview

An overview of DR is presented. The equation of motion governing the absorber dynamics (Fig. 1b) is

$$m_a\ddot{x}_a(t) + c_a\dot{x}_a(t) + k_a x_a(t) - g\ddot{x}_a(t-\tau) = 0 \qquad \text{(A1)}$$

where the last term represents the delayed acceleration feedback. The Laplace domain transformation of this equation yields the characteristics equation

$$m_a s^2 + c_a s + k_a - g s^2 e^{-\tau s} = 0 \qquad \text{(A2)}$$

Without feedback ($g = 0$) this structure is dissipative with two characteristic roots (poles) on the left half of the complex plane. For g

and $\tau > 0$, however, these two finite stable roots are supplemented by infinitely many additional finite roots. Note that these characteristic roots (poles) of Eq. (A2) are discretely located (for instance, at $s = a + j\omega$), and the following relation holds:

$$g = \left(\left|m_a s^2 + c_a s + k_a\right| / |s^2|\right) e^{\tau a} \tag{A3}$$

where $|\cdot|$ denotes the magnitude of the argument.

With Eq. (A3), the following observations can be made:

1) For $g = 0$, there are two finite stable poles and all remaining poles are at $a = -\infty$.

2) For $g = +\infty$, there are two poles at $s = 0$, and the rest are at $a = +\infty$.

When we consider these observations and take into account the continuity of the root loci for a given delay τ, and as g varies from 0 to ∞, it is obvious that the roots of Eq. (A2) move from stable left half to the unstable right half of the complex plane. For a certain critical gain g_c, one pair of poles reaches the imaginary axis. At this operating point, the DR becomes a perfect resonator, and the imaginary characteristic roots are $s = \pm j\omega_c$, where ω_c is the resonance frequency and $j = \sqrt{-1}$. The subscript c implies the crossing of the root loci on the imaginary axis. The control parameters g_c and τ_c of concern can be found by substitution of the desired $s = \pm j\omega_c$ into Eq. (A2) as

$$g_c = \frac{1}{\omega_c^2}\sqrt{(c_a\omega_c)^2 + \left(m_a\omega_c^2 - k_a\right)^2}$$

$$\tau_c = \frac{1}{\omega_c}\left\{\tan^{-1}\left[\frac{c_a\omega_c}{m_a\omega_c^2 - k_a}\right] + 2(\ell - 1)\pi\right\}, \qquad \ell = 1, 2, \ldots \tag{A4}$$

When these g_c and τ_c are used the DR structure (Fig. 1b) mimics a resonator at frequency ω_c. In turn, this resonator forms an ideal absorber of tonal vibration at ω_c. The objective of the control, therefore, is to maintain the DR absorber at this marginally stable point. Further discussions on the DR stability can be found in Refs. 6 and 12.

Appendix B: BFGS Direct Update Method

An initial vector $\boldsymbol{X}^{(0)}$ is selected that contains all parameters over which the optimization is carried out. A symmetric positive definite matrix $\boldsymbol{H}^{(0)}$ as an estimate for the Hessian of the objective function $F(\boldsymbol{X})$ is then chosen. In the absence of further information, $\boldsymbol{H}^{(0)} = \boldsymbol{I}$ is assumed. In the next step, the gradient vector of the objective function is calculated as

$$\boldsymbol{C}^{(0)} = \nabla F\left(\boldsymbol{X}^{(0)}\right) \tag{B1}$$

Then, the following linear system of equations is solved to obtain the search direction $\boldsymbol{d}^{(k)}$

$$\boldsymbol{H}^{(k)}\boldsymbol{d}^{(k)} = -\boldsymbol{C}^{(k)} \tag{B2}$$

starting from $k = 0$. The absorber parameters are then updated as

$$\boldsymbol{X}^{(k+1)} = \boldsymbol{X}^{(k)} + a_k\boldsymbol{d}^{(k)} \tag{B3}$$

where the scalar $a_k = a$ is the step size along the search direction, which minimizes $G(\boldsymbol{X}^{(k)} + a\boldsymbol{d}^{(k)})$. It is computed using any one-dimensional search method, such as the golden section search method[17] we selected for this work. The Hessian approximation for the objective function is updated according to the following rule, the proof of which is in Ref. 16:

$$\boldsymbol{H}^{(k+1)} = \boldsymbol{H}^{(k)} + \boldsymbol{D}^{(k)} + \boldsymbol{E}^{(k)} \tag{B4}$$

where the correction matrices $\boldsymbol{D}^{(k)}$ and $\boldsymbol{E}^{(k)}$ are given as

$$\boldsymbol{D}^{(k)} = \frac{\boldsymbol{u}^{(k)}\boldsymbol{v}^{(k)^T}}{\left(\boldsymbol{u}^{(k)} \cdot \boldsymbol{v}^{(k)}\right)}, \qquad \boldsymbol{E}^{(k)} = \frac{\boldsymbol{C}^{(k)}\boldsymbol{C}^{(k)^T}}{\left(\boldsymbol{C}^{(k)} \cdot \boldsymbol{d}^{(k)}\right)} \tag{B5}$$

with

$$\boldsymbol{v}^{(k)} = a_k\boldsymbol{d}^{(k)}(\text{change in parameters})$$

$$\boldsymbol{u}^{(k)} = \boldsymbol{C}^{(k+1)} - \boldsymbol{C}^{(k)}(\text{change in gradient})$$

$$\boldsymbol{C}^{(k+1)} = \nabla F\left(\boldsymbol{X}^{(k+1)}\right) \tag{B6}$$

The procedure repeated for $k = k + 1$, until the following inequality is satisfied:

$$\left\|\boldsymbol{C}^{(k)}\right\| < \varepsilon \tag{B7}$$

where $\varepsilon > 0$ is a small convergence parameter that is selected by the user.

This unconstrained optimization procedure is also applicable to constrained problems. In that case the objective function F needs to be modified as (see Ref. 17)

$$F_{\text{new}}(\boldsymbol{X}, \boldsymbol{r}) = F(\boldsymbol{X}) + Q[\boldsymbol{h}(\boldsymbol{X}), \boldsymbol{r}] \tag{B8}$$

where $\boldsymbol{r}$ is a vector of penalty-imposing parameters and $\boldsymbol{h} = \{h_i(\boldsymbol{X})\}$, where $i = 1, 2, \ldots, m$, is the set of m inequality constraints. Q is a real-valued function whose contribution to the objective function F_{new} is controlled by $\boldsymbol{r}$. Here we use the inverse barrier function for Q as[17]

$$Q[\boldsymbol{h}(\boldsymbol{X}), r] = \left(\frac{1}{r}\right)\sum_{i=1}^{m}\left[\frac{-1}{h_i(\boldsymbol{X})}\right] \tag{B9}$$

where r is taken as a positive scalar.

References

[1] Sun, J. Q., Jolly, M. R., and Norris, M. A., "Passive, Adaptive, and Active Tuned Vibration Absorbers—A Survey," *ASME Transactions*, Special 50th Anniversary Design Issue, Vol. 117, 1995, pp. 234–242.

[2] Puksand, H., "Optimum Conditions for Dynamic Vibration Absorbers for Variable Speed Systems with Rotating and Reciprocating Unbalance," *International Journal of Mechanical Engineering Education*, Vol. 3, 1975, pp. 145–152.

[3] Jacquot, R. G., "Optimal Dynamic Vibration Absorbers for General Beam," *Journal of Sound and Vibration*, Vol. 60, No. 4, 1978, pp. 535–542.

[4] Warburton, G. B., and Ayorinde, E. O., "Optimum Absorber Parameters for Simple Systems," *Earthquake Engineering and Structural Dynamics*, Vol. 8, 1980, pp. 197–217.

[5] Manikanahally, D. N., and Crocker, M. J., "Vibration Absorbers for Hysteretically Damped Mass-Loaded Beams," *Journal of Vibration and Acoustics*, Vol. 113, 1991, pp. 116–122.

[6] Olgac, N., and Holm-Hansen, B., "A Novel Active Vibration Absorption Technique: Delayed Resonator," *Journal of Sound and Vibration*, Vol. 176, 1994, pp. 93–104.

[7] Olgac, N., "Delayed Resonators as Active Dynamic Absorbers," U.S. Patent 5,431,261, July 1995.

[8] Jalili, N., and Olgac, N., "Optimum Delayed Feedback Vibration Absorber for MDOF Mechanical Structures," *Proceedings of 37th IEEE Conference on Decision Control*, IEEE Publications, Piscataway, NJ, 1998, pp. 4734–4739.

[9] Renzulli, M., Ghosh-Roy, R., and Olgac, N., "Robust Control of the Delayed Resonator Vibration Absorbers," *Proceedings of 3rd ARO Workshop on Smart Structures*, 1997.

[10] Bapat, V. A., and Kumaraswamy, H. V., "Effect of Primary System Damping on the Optimum Design of an Untuned Viscous Dynamic Vibration Absorber," *Journal of Sound and Vibration*, Vol. 63, 1979, pp. 469–474.

[11] Rao, S. S., *Mechanical Vibrations*, 3rd ed., Addison Wesley Longman, New York, 1995, pp. 603–914.

[12] Olgac, N., Elmali, H., Hosek, M., and Renzulli, M., "Active Vibration Control of Disturbed Systems Using Delayed Resonator with Acceleration Feedback," *Journal of Dynamic Systems, Measurement and Control*, Vol. 119, 1997, pp. 380–388.

[13] Filipovic, D., and Olgac, N., "Torsional Delayed Resonator with Velocity Feedback," *IEEE/ASME Transactions on Mechatronics*, Vol. 3, No. 1, 1998, pp. 67–72.

[14] Kolmanovski, V. B., and Nosov, V. R., *Stability of Functional Differential Equations*, Academic, London, 1989.

[15] Ackermann, J., *Robust Control, Systems with Uncertain Physical Parameters*, Springer-Verlag, Berlin, 1993.

[16] Gill, P. E., Murray, W., and Wright, M. H., *Practical Optimization*, Academic, New York, 1981.

[17] Arora, J. S., *Introduction to Optimum Design*, McGraw–Hill, New York, 1989, pp. 330–340.